Hindawi
Journal of Chemistry
Volume 2020, Article ID 1474357, 13 pages
https://doi.org/10.1155/2020/1474357

Research Article

Heterogeneous UV/Fenton-Like Degradation of Methyl Orange Using Iron Terephthalate MIL-53 Catalyst

Pham Dinh Du,[1] **Huynh Thanh Danh**,[2] **Pham Ngoc Hoai**,[1] **Nguyen Mau Thanh**,[3] **Vo Thang Nguyen**,[4] **and Dinh Quang Khieu**[5]

[1]*Thu Dau Mot University, Thu Dau Mot 75000, Vietnam*
[2]*Giong Rieng High School, Giong Rieng 91000, Vietnam*
[3]*Quang Binh University, Dong Hoi 47000, Vietnam*
[4]*The University of Da Nang, University of Science and Education, Da Nang 50000, Vietnam*
[5]*University of Sciences, Hue University, Hue 49000, Vietnam*

Correspondence should be addressed to Dinh Quang Khieu; dqkhieu@hueuni.edu.vn

Received 5 February 2020; Revised 24 April 2020; Accepted 18 May 2020; Published 12 June 2020

Guest Editor: Tapan Sarkar

The synthesis and degradation of methyl orange (MO) in an ultraviolet-assisted heterogeneous Fenton-like process via the iron terephthalate (MIL-53) catalyst are demonstrated. MIL-53 material was characterized by means of X-ray diffraction (XRD), Fourier-transform infrared spectroscopy (FT-IR), UV-Vis diffuse reflectance spectra (DR-UV-Vis), X-ray photoelectron spectroscopy (XPS), scanning electron microscopy (SEM), and nitrogen adsorption/desorption isotherms. It was found that the obtained material shares an identical pattern of the MIL-53 structure with high crystallinity and also demonstrates the mesoporous phase with a pore diameter of around 4.2 nm and specific surface area, S_{BET}, of 88.2 $m^2 \cdot g^{-1}$. MIL-53 with UV irradiation exhibits high catalytic activity for MO degradation by hydrogen peroxide. The factors affecting the efficiency of MO decomposition including pH of the solution, H_2O_2 concentration, catalyst dosage, initial MO concentration, and reaction temperature were addressed. The present catalyst is stable after four recycles with slight catalytic activity loss which makes it a potential candidate for environmental restoration.

1. Introduction

tWater pollution by dyes and pigments is a concern for the development of communities. A better approach to remove dyes and pigments from wastewater has become a major research focus in the field of water treatment because water contaminated with dyes and pigments, even at very low concentrations, can cause many negative impacts on the aquatic environment [1]. Moreover, many dyes are found to be structurally stable and cannot be easily decomposed by sunlight irradiation, chemical agents, or biological agents and can affect human health [2]. There is evidence that the biodegradation of dyes in wastewater using conventional biological methods is negligible; therefore, wastewater containing high levels of dyes is usually treated by physical or chemical methods, such as coagulation and flocculation [3], oxidation or ozonation [4, 5], membrane filtration [6], and adsorption [7].

Currently, the advanced oxidation processes (AOPs) are considered to be an effective green method for treating wastewater containing organic substances/dyes. Among AOPs, Fenton and Fenton-like oxidations have been commonly used to produce $OH^{\bullet}$ radicals via catalyzing H_2O_2 by ferrous ions in acidic media [8]. Fenton-like processes are treatment procedures involving the *in situ* generation of the active hydroxyl radical ($OH^{\bullet}$) that has a high standard potential ($E^{\circ} = 2.80$ V/SHE) and can nonselectively oxidize almost all organic compounds into CO_2, H_2O, and inorganic ions [9, 10]. This is a suitable and highly effective technology to decompose persistent organic pollutants [11]. The Fenton reaction is amongst the AOPs proving its efficiency with the use of a minimum amount of precursors. Furthermore, all

transition metals employed in the Fenton system are environmentally friendly.

The classical Fenton reaction is described by the activation of hydrogen peroxide (H_2O_2) with ferrous ions (Fe^{2+}) to form hydroxyl radicals ($OH^{\bullet}$) via the following equation [12]:

$$Fe^{2+} + H_2O_2 \longrightarrow Fe^{3+} + HO^{\bullet} + OH^{-} \left(k = 63 - 76\,M^{-1} \cdot s^{-1}\right) \quad (1)$$

Fe^{2+} ions will be regenerated when Fe^{3+} reacts with the remaining H_2O_2 as described in the following equation:

$$Fe^{3+} + H_2O_2 \longrightarrow Fe^{2+} + H^{+} + HO_2^{\bullet} \left(k = 0.001 - 0.01\,M^{-1} \cdot s^{-1}\right) \quad (2)$$

Recently, it has been shown that the Fenton process can be further enhanced with UV light illumination [12, 13], which can be explained by an increase in $OH^{\bullet}$ radical production due to the decay of the photoactive $Fe(OH)^{2+}$ moiety and H_2O_2 under the following condition:

$$Fe(OH)^{2+} + h\nu \longrightarrow Fe^{2+} + HO^{\bullet}$$
$$H_2O_2 + h\nu \longrightarrow 2^{HO\bullet} \quad (3)$$

However, this homogeneous Fenton catalytic procedure requires a concentration of 50–80 ppm of iron, which is much larger than allowable level (the standard of 2 ppm guided by European Community Directives) [13]. Therefore, the removal of iron ions in the already treated solution has to be taken into account with suitable additional techniques, which consequently has led to a rise in operational cost. This motivates the development of heterogeneous Fenton-like processes. The catalysts for these systems include iron or transition metal containing solids in which the catalytic mechanisms are similar to homogeneous Fenton catalytic one, but only the reactions which occur on the surface of heterogeneous catalysts in this way limit the disadvantage of homogeneous catalysts [8–10].

Many studies have investigated the use of various inorganic and organic materials as a supportive matrix for active iron ions in the heterogeneous Fenton-like process, such as SBA-15 [13], carbon [14], kaolin [15], and MCM-41 [16]. As an iron-containing solid, iron oxide nanoparticle is amongst the candidates to act as a catalyst in heterogeneous Fenton systems for decoloring and mineralization of various dyes or organic substances [17, 18].

The metal-organic framework (MOF) materials are characteristic by larger specific surface area, high porosity, and perfect binding structure, which have attracted much scientific attention in the fields of gas separation or storage, molecular sensors, and catalysts [19–24]. MOFs also demonstrate semiconductor properties under appropriate lighting conditions, which means that they have potential to be applied in the photocatalytic field [21]. MIL-53 (MIL: Material Institute Lavoisier) is a porous MOF with a three-dimensional structure constructed from -Fe-O-O-Fe-O-Fe- bridges with bis-bidentate terephthalate (1,4-benzenedicarboxylate) linkers. MIL-53 contains ferrous transition metal that acts as catalytic sites and is considered to have photocatalytic activity [21]. Therefore, it can also be utilized as a catalyst in the heterogeneous Fenton-like system. To the best of our knowledge, few heterogeneous UV/Fenton-like processes with MIL-53 have been reported.

In this paper, MIL-53 was synthesized by the hydrothermal method. Some factors affecting the formation of MIL-53 have been studied. The heterogeneous UV/Fenton-like system using the MIL-53 catalyst for methyl orange degradation has been addressed.

2. Experimental

2.1. Materials. Iron chloride hexahydrate ($FeCl_3.6H_2O$, 99.1%, Merck, Code 1039430250, EMD Millipore Corporation, Germany), terephthalic acid ($C_8H_6O_4$, 99%, Acros, Code 180722500, Janssen Pharmaceuticalaan, Belgium) (denoted as TA), N'N-dimethylformamide (C_3H_7NO, ≥99.5%, Fisher, Code D/3841/15, Leicestershire, England) (denoted as DMF), and methyl orange ($C_{14}H_{14}N_3NaO_3S$, Merck, Germany) (denoted as MO) were used in this study.

2.2. MIL-53 Synthesis. Iron-terephthalate organic-inorganic hybrid material was prepared in a similar manner as reported by Du et al. with some modifications [21]. In this procedure, the mixture of 1.2469 g of $FeCl_3{\cdot}6H_2O$, 0.7663 g of TA, and 160 mL of DMF was mixed in a Teflon-lined steel autoclave (volume of 200 mL) and heated in an oven at different temperatures for 24 hours. The solid product (yellowish brown powder) was then filtered out and dried overnight at 150°C. After cooling down to room temperature, the solid was washed with distilled water (1 g of the material with 0.5 L of water), filtered, and dried to obtain the MIL-53(Fe) catalyst. In order to study the effect of molar ratio of $FeCl_3$/TA and reaction temperature on the formation of the MIL-53 phase, each of these parameters was varied when fixing other parameters at specific values, including reaction time of 24 hours and DMF solvent volume of 160 mL. In detail, molar ratio of $FeCl_3$/TA was varied from 1 : 1, 1 : 2 to 1 : 3 at a temperature of 150°C, and reaction temperature was raised from 100 to 180°C at a molar ratio of $FeCl_3$/TA of 1 : 2.

2.3. Characterization. X-ray diffraction (XRD) patterns were recorded on a VNU-D8 Advance Instrument (Bruker, Germany) under Cu Kα radiation ($\lambda = 1.5406$ Å). The N_2 adsorption/desorption isotherm measurement test was performed at 77 K in a Tristar 3000 analyzer, and before setting the dry mass, the samples were degassed at 250°C with N_2 for 5 h. Scanning electron microscopy (SEM) images were obtained using SEM JMS-5300LV (Japan), and Fourier-transform infrared spectra (FT-IR) were recorded in a Jasco FT/IR-4600 spectrometer (Japan) in the range of 4,000–400 cm^{-1}. X-ray photoelectron spectroscopy (XPS) was conducted using a Shimadzu Kratos AXIS Ultra DLD spectrometer (Japan). Peak fitting was performed by CasaXPS software. UV-Vis diffuse reflectance data were collected over the spectral range 200–800 nm with the UV2600 Shimadzu (Japan) spectrophotometer equipped

with an integrated sphere, and $BaSO_4$ was used as a reference sample. To evaluate the mineralization of MO, total organic carbon (TOC) was measured using a Shimadzu TOC-V_{CPH} analyzer.

2.4. Catalytic Activity of MIL-53. The decomposition of MO was carried out with the presence of the MIL-53 catalyst and hydroperoxide. In each experiment, 0.05 g of the catalyst was suspended in 100 mL containing MO at a specific concentration and 0.192 M H_2O_2 in a 500 mL reactor with a reflux condenser. The solution was stirred vigorously under UV irradiation. 3 mL of the solution was withdrawn at regular time intervals and centrifuged to remove the catalyst. The MO concentration in the supernatant was determined by the UV-Vis method on Jasco V-770 (Japan) at $\lambda_{max} = 465$ nm. Other experiments were also carried out without the presence of the catalyst and without irradiation for the sake of comparison.

In addition, the products of the MO oxidation reaction by hydroperoxide over time were also evaluated by the HPLC method on the UFLC Shimadzu (Japan) equipment. The HPLC was equipped with the C-18 column using the ammonium acetate 10 mM : methanol = 3 : 7 mobile phase and the SPD-20A detector at a wavelength of 254 nm.

3. Results and Discussion

3.1. Catalyst Characterization

3.1.1. XRD and SEM. The samples synthesized at various molar ratios of $FeCl_3$/TA, 1 : 1, 1 : 2, and 1 : 3, were analyzed by X-ray diffraction, and the XRD patterns are shown in Figure 1. At a molar ratio of $FeCl_3 : TA = 1 : 1$, the sample exhibits characteristic diffraction peaks for iron oxide (Fe_2O_3) at 24.08, 33.17, 35.57, 40.79, 49.37, 54.02, 57.56, and 62.42° according to JCPDS card no. 01-089-0598 (Figure 1(a)) and for MIL-53, at 9.29, 10.85, 17.18, and 21.95° [25–27]. This result indicates the coexistence of the MIL-53 material and iron oxide. At a higher amount of TA, i.e., molar ratio $FeCl_3 : TA = 1 : 2$ and 1 : 3, the diffraction peaks appear at 2θ of 9.17, 12.59, 17.51, 18.17, 18.47, and 25.37°, being consistent with the previous publications on the MIL-53 material [21, 25–27], and no diffraction peaks of iron oxide can be observed. This confirms that MIL-53 has been formed at these molar ratios with high purity (Figure 1(b)). The XRD pattern of MIL-53 sample synthesized by FeCl3/TA molar ratio of 1/2 possesses highest intensity and maximum sharpness, indicating that the obtained MIL-53 material exhibits highly ordered structure and high crystallinity.

The XRD patterns of MIL-53 synthesized at different hydrothermal temperatures are also shown in Figures 1(c) and 1(d). The samples synthesized at temperatures of 100, 120, and 150°C exhibit diffraction peaks which are typical for the MIL-53 structure. However, the synthetic sample at 180oC shows the characteristic diffraction peaks for iron oxide (JCPDS card no. 01-089-0599) (Figure 1(d)). Therefore, $FeCl_3$/TA molar ratio of 1/2 and the hydrothermal temperature of 150°C were chosen to synthesize the MIL-53 material.

The SEM images (Figure 2) reveal the morphology of the MIL-53 sample synthesized at the $FeCl_3$/TA molar ratio of 1 : 1 and 1 : 2 at the hydrothermal temperature of 150°C. The sample synthesized at the molar ratio of $FeCl_3 : TA = 1 : 1$ presents the morphology with irregular particles (sphere and rod shapes) (Figures 2(a) and 2(b)). Meanwhile, the molar ratio of $FeCl_3 : TA = 1 : 2$ led to the formation of materials of highly crystalline polyhedron rods with relatively uniform and smooth surfaces and sharp edges (Figures 2(c) and 2(d)). This is also in good agreement with the XRD results where sharp diffraction and high intensity peaks are observed. Therefore, the molar ratio of $FeCl_3 : TA = 1 : 2$ was selected for further investigations.

3.1.2. FT-IR and XPS Spectroscopy. Terephthalic acid (TA) and the obtained MIL-53 samples were also characterized by FT-IR spectra (Figure 3). The spectrum of TA exhibits characteristic absorption bands in which the typical peaks are C=O stretching vibration (1681 cm^{-1}), OH bending vibration (1,423 and 937 cm^{-1}), and C-H bending vibration of the benzene ring (784 cm^{-1}) [28]. The MIL-53 samples synthesized at 100°C and 120°C present the typical vibrational bands of the carboxylic acid function in the region of 500–1,750 cm^{-1} indicating the presence of terephthalic acid residual, and the formation of the MIL-53 phase is incomplete at these temperatures. Meanwhile, at the temperature of 150°C, it clearly shows the disappearance of the characteristic band for the carboxyl group at 1,681 cm^{-1} and the formation of the absorption band for the ligand coordinated to the metal centers in MIL-53 at 1,523 cm^{-1}. In addition, the peak at 537 cm^{-1}, respectively, corresponding to the vibration of ν(Fe-O) stretching reveals the formation of the metal-oxo bond between the carboxylic group of terephthalic acid and Fe(III) [26]. Such differences manifest the absence of the free ligand in as-synthesized MIL-53. At high hydrothermal temperature of 180°C, the characteristic vibration of MIL-53 can be hardly observed, with the only apparent peak at 537 cm^{-1} of ν(Fe-O) stretching vibration. This additional evidence confirms that hydrothermal temperature at 150°C is appropriate for the formation of the MIL-53 material.

The elemental composition and the electronic structure of the MIL-53 sample were analyzed by XPS spectroscopy. The XPS survey spectrum of the obtained MIL-53(Fe) (Figure 4(a)) confirms the presence of Fe, C, and O elements on the surface of the sample. Figure 4(b) shows the high-resolution XPS spectrum of Fe2p with two peaks with the binding energy of 710 eV and 723 eV assigned to $Fe2p_{3/2}$ and $Fe2p_{1/2}$ of Fe(III), respectively [26]. The XPS spectrum of C2s (Figure 4(c)) exhibits three peaks at 284.7 eV, 288.6 eV, and 286.5 eV corresponding to carbon components on the benzoic ring, the carboxylate group (O-C=O) of the terephthalate bridges [26], and the C-O bond [29]. The XPS spectrum of O1s shows three peaks with the binding energy of 529.9, 531.8, and 533.1 eV (Figure 4(d)). The two former peaks can be attributed to the oxygen component on the

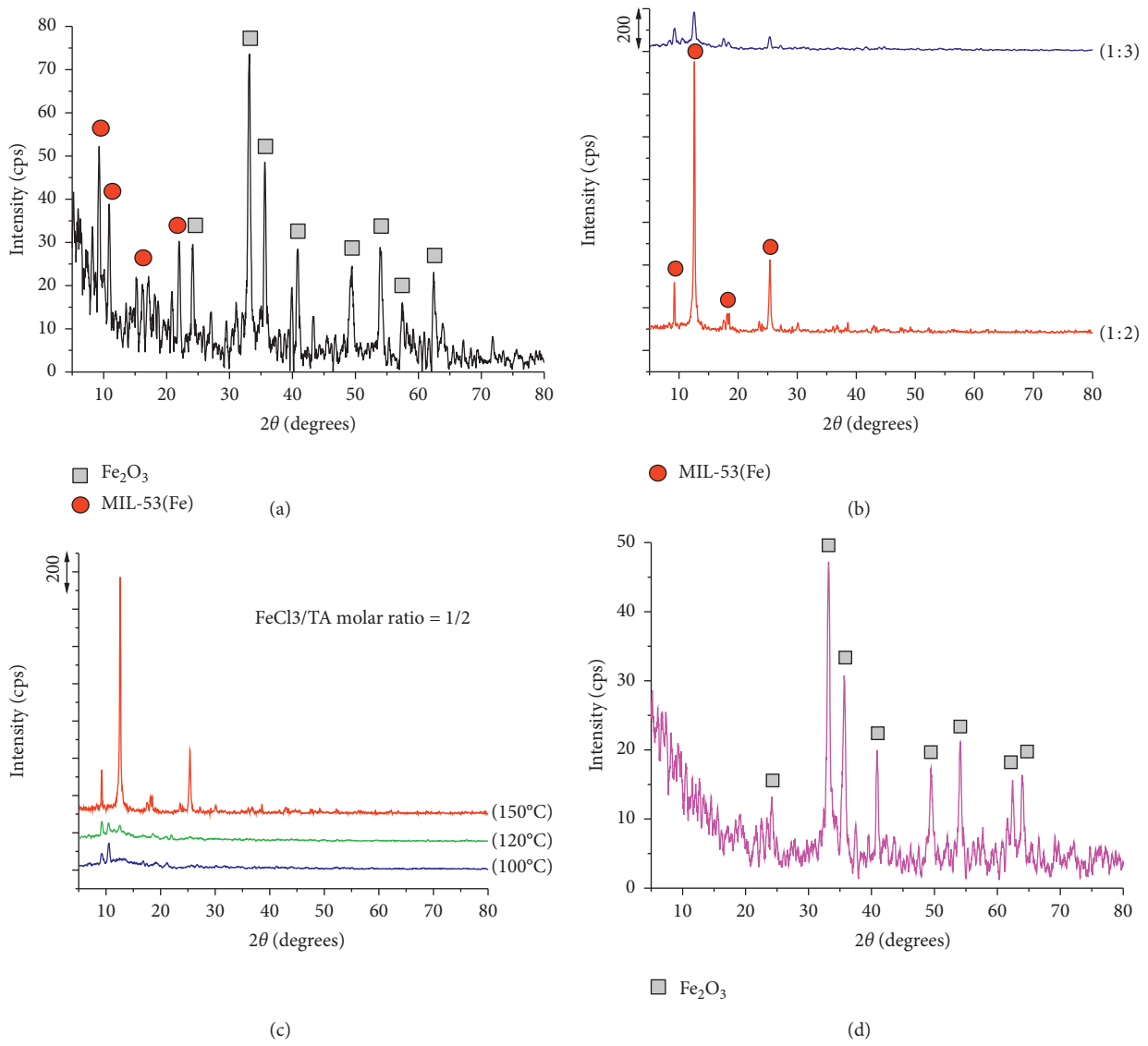

Figure 1: XRD patterns of MIL-53 samples synthesized at the hydrothermal temperature of 150°C: (a) $FeCl_3$/TA molar ratio of 1/1; (b) $FeCl_3$/TA molar ratio of 1/2 and 1/3; MIL-53 samples with an $FeCl_3$/TA molar ratio of 1/2 synthesized at the hydrothermal temperature of (c) 100, 120, and 150°C; (d) 180°C.

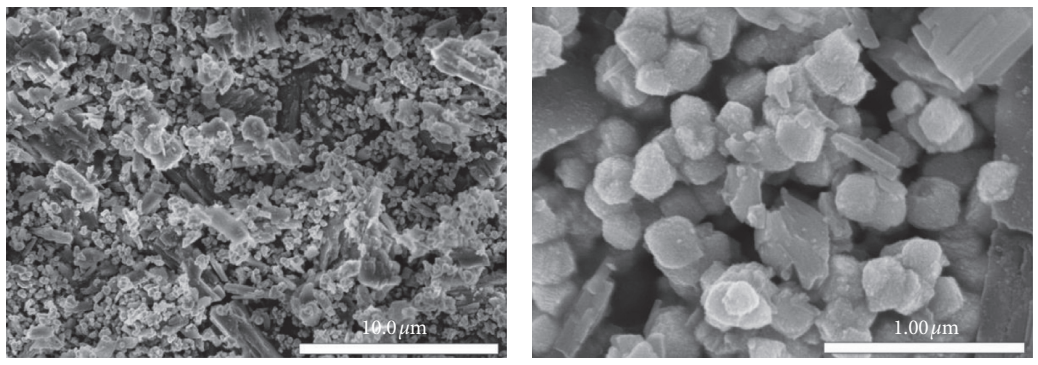

(a) (b)

Figure 2: Continued.

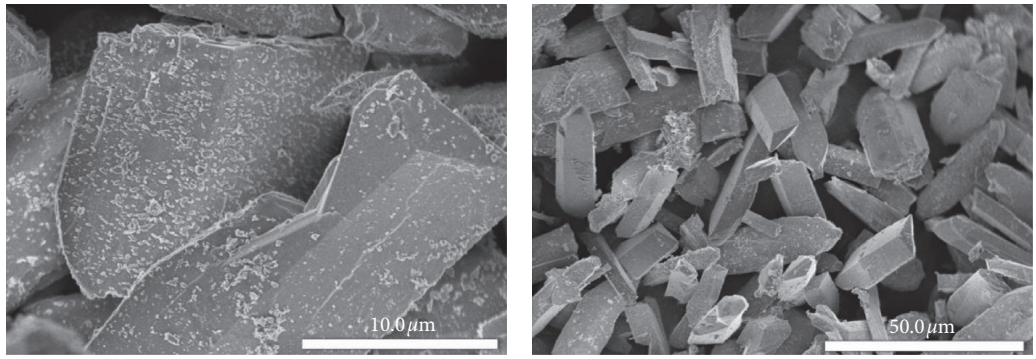

(c) (d)

Figure 2: SEM images with different magnifications of the MIL-53 samples: the $FeCl_3$/TA molar ratio of 1 : 1 (a and b) and 1 : 2 (c and d).

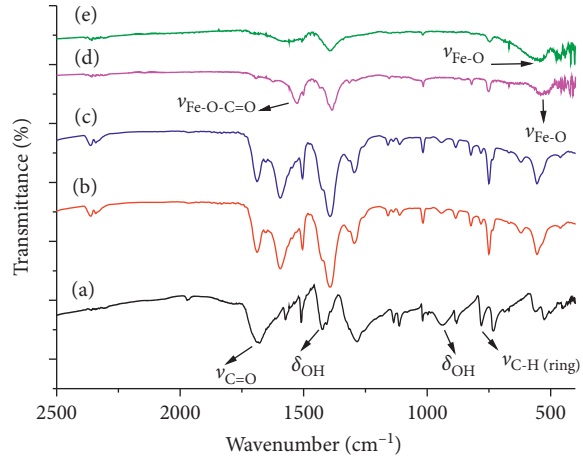

Figure 3: FT-IR spectrum of terephthalic acid (a); FT-IR spectra of MIL-53 samples synthesized at the temperature of 100°C (b), 120°C (c), 150°C (d), and 180°C (e) ($FeCl_3$: TA molar ratio of 1 : 2).

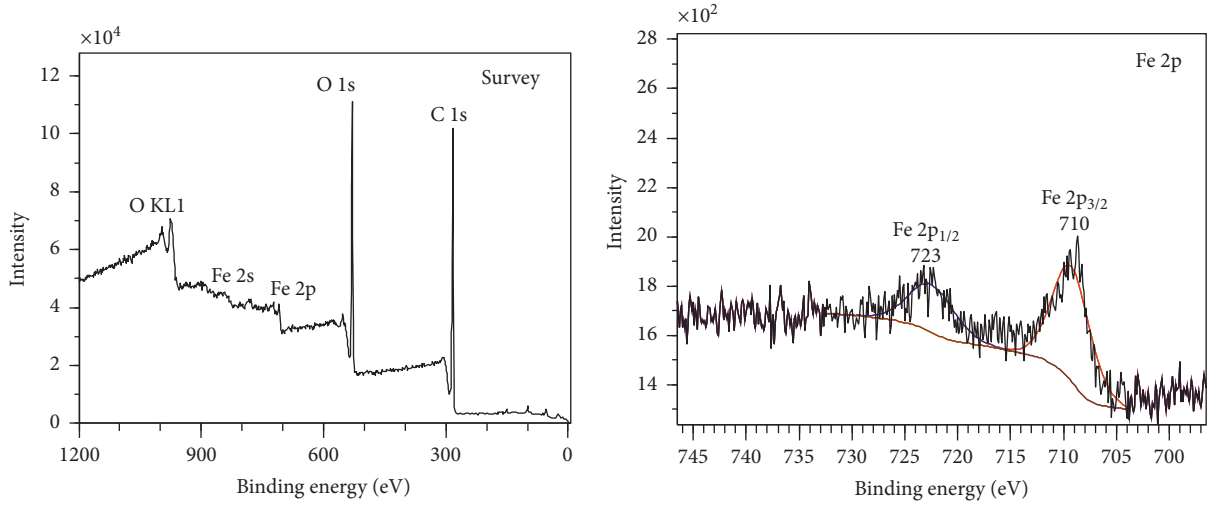

Figure 4: Continued.

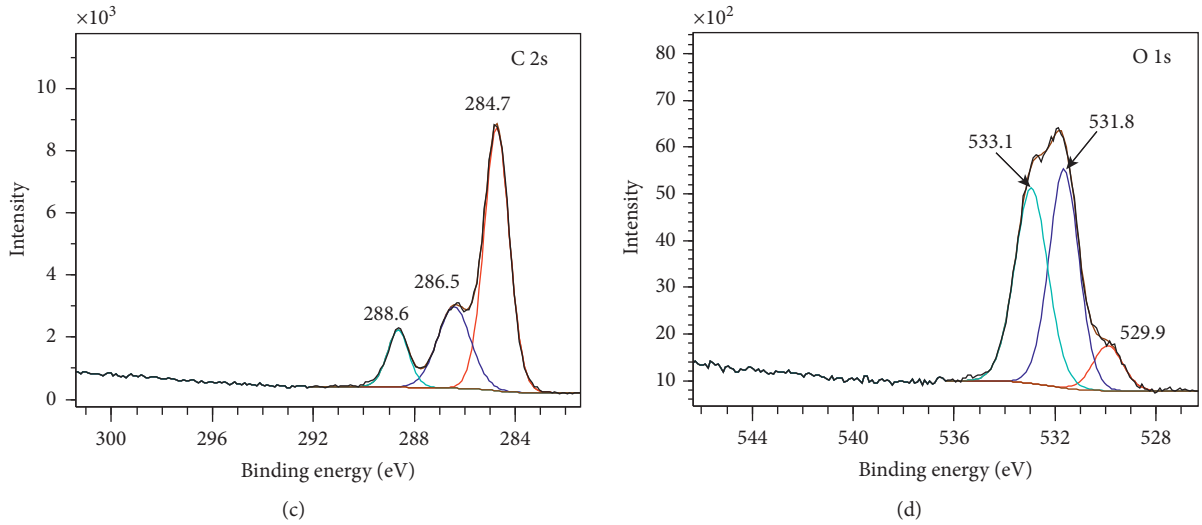

FIGURE 4: XPS spectra of the MIL-53(Fe) sample synthesized at the molar ratio $FeCl_3$: TA = 1 : 2 and hydrothermal temperature of 150°C: (a) survey spectrum; (b) Fe2p; (c) C2s; (d) O1s.

terephthalate bridges and Fe-O bonds of MIL-53(Fe) [26], while the latter peak at 533.1 eV is assigned to the adsorbed water molecules on the surface of the material [29].

3.1.3. UV-Vis Diffuse Reflectance Spectrum and Nitrogen Adsorption-Desorption Isotherms. The UV-Vis diffuse reflectance spectrum of MIL-53 is shown in Figure 5(a). There are two absorption bands peaked at 395 and 450 nm, corresponding to the energy gap value, E_g of 2.4 and 1.9 eV (Figure 5(b)), both of which are lower than the value of 2.8 eV that Du et al. [21] published on the MIL-53 material. This suggests that the obtained sample may have photocatalytic activity.

The nitrogen adsorption-desorption isotherms of MIL-53 follow type II profile with a hysteresis of H3 type according to IUPAC classification (Figure 5(c)). The obtained sample demonstrates a highly ordered porous distribution with a diameter of about 4.2 nm (Figure 5(d)). The specific surface area determined by the BET equation of the MIL-53 sample is 88.2 m^2/g, which is much higher than that reported in the previous literature (14 m^2/g) [30].

3.2. Catalytic Activities

3.2.1. Methyl Orange Degradation without the Catalyst. The decomposition of methyl orange (MO) under different conditions (UV irradiation and hydroperoxide as the oxidative agent) but without the catalyst is presented in Figure 6. From the figure, the MO concentration seems unchangeable as UV was irradiated even for 240 minutes indicating MO is stable in this condition. The MO concentration is reduced slightly (around 8.3%) when the mixture of MO and hydroperoxide was stirred for 240 minutes. It is worth noting that the combination of hydroperoxide and UV irradiation significantly enhanced the removal of MO when MO concentration reduces significantly from 10 to 3.92 mg/L (around 60.8%) after 240 minutes. The faster decomposition of MO can be assigned to the synergistic effect of the UV photon energy on increasing the rate of H_2O_2 decomposition to produce free radical $OH^{\bullet}$, which in turn increases the reaction rate of MO oxidation.

3.2.2. Methyl Orange Degradation in the Presence of the MIL-53 Catalyst. Decolorization of the MO solution in the presence of MIL-53 under different conditions is presented in Figure 7(a). It was found that the MO degradation over MIL-53 solely was insignificant, only 19% after 240 minutes. However, the MIL-53 material exhibited high catalytic activity in the presence of the H_2O_2 agent as the heterogeneous Fenton-like system in which 68.3% of MO was decomposed after 240 minutes. It is worth noting that the UV radiation markedly accelerates MO degradation. When UV light was irradiated to the reaction mixture containing H_2O_2 and MIL-53, MO was removed completely after only 60 minutes of the reaction. This rapid reaction may be due to the combination of heterogeneous Fenton-like reactions and the enhanced decomposition of H_2O_2 under UV radiation. Therefore, the MO decomposition reaction in the aqueous solution was carried out in the heterogeneous UV/Fenton-like system with the MIL-53 catalyst in the subsequent investigations.

A leaching experiment was also conducted by continuing monitoring the solution after filtering out the MIL-53 catalyst by centrifugation at 20 min of the reaction (Figure 7(b)). It is clear that the removal of dye was quenched despite the fact that UV light irradiation was still maintained in the presence of H_2O_2. This indicates that there was no leaching of iron species into the reaction solution from the heterogeneous catalyst. The above experimental results confirmed that MIL-53 acts as a heterogeneous catalyst in the MO degradation process.

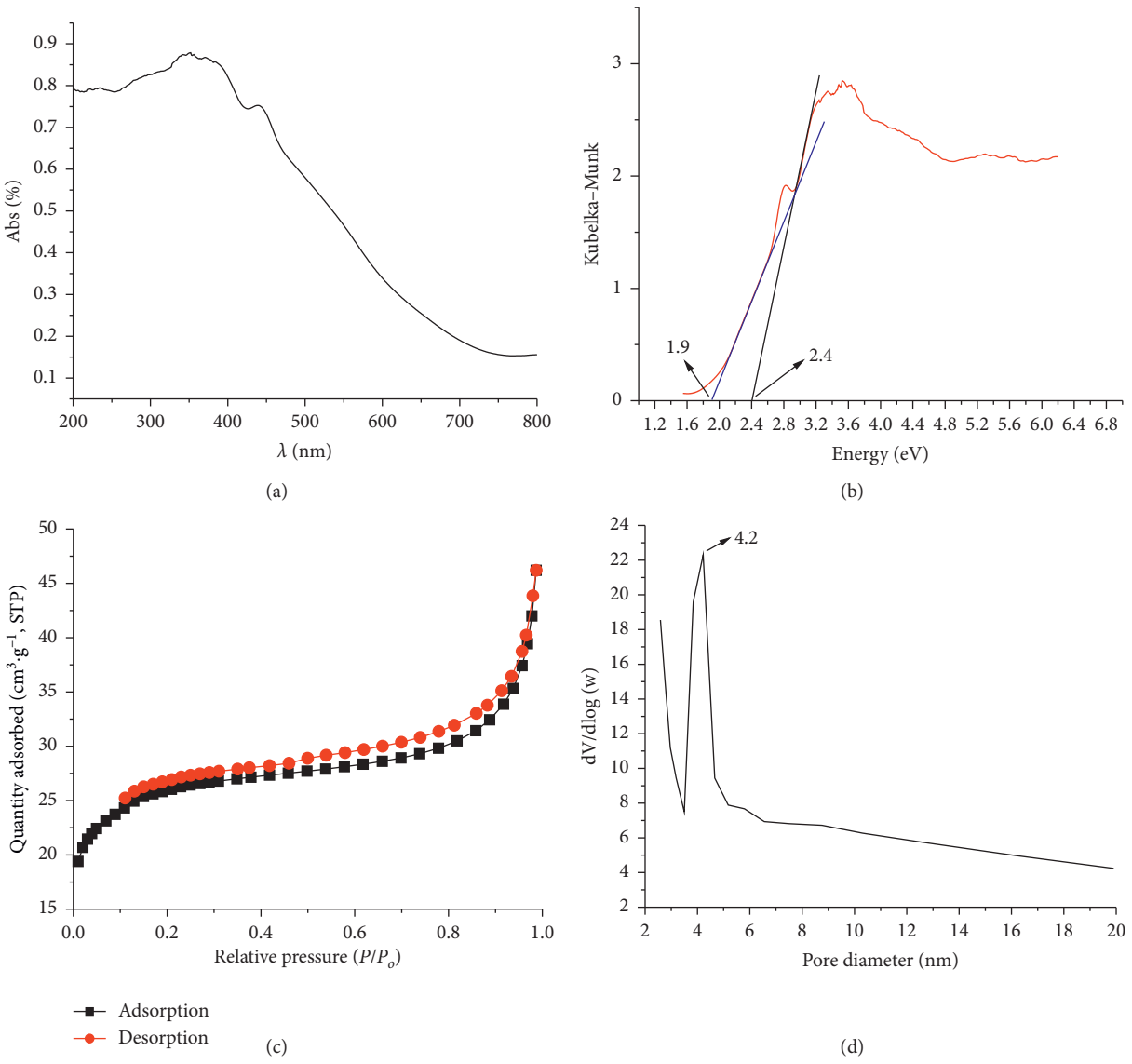

Figure 5: (a) UV-Vis diffuse reflectance spectrum, (b) the plot of Kubelka–Munk function versus the energy of absorbed light, (c) nitrogen adsorption-desorption isotherms, and (d) pore size distribution of the MIL-53 sample ($FeCl_3$/TA molar ratio = 1 : 2 at the hydrothermal temperature 150°C).

3.2.3. Methyl Orange Decomposition Reaction by the MIL-53 Catalyst in the UV/Heterogeneous Fenton-Like System

(1) Effect of Solution pH. The efficiency of MO degradation in the presence of the MIL-53 catalyst at different pH is shown in Figure 8. It was found that, at pH 2, the decomposition of MO was significantly superior when it took 70 minutes for MO to be totally decomposed. Upon increasing pH, there were two stages in the decomposition profile in which the reaction occurred slowly in the first 30 minutes and was accelerated thereafter. It is interesting that the trend for MO decomposition was similar in a pH range of 4 to 8, and MO was completely decomposed after 90 minutes of the reaction. As pH increased from 9 to 12, the rate of MO decomposition decreased when the loss of MO decreased from 86% to 47% after 120 minutes of the reaction. The reduction of MO degradation at high pH can be explained by the instability of H_2O_2 and the low oxidation ability of the hydroxyl radical in the alkaline environment [31]. This result proves that the MIL-53 material can be used as a catalyst in a wide pH range (2–12) implying that this is a heterogeneous Fenton-like catalytic system.

(2) Effect of H_2O_2 Dosage. Figure 9 shows the effect of H_2O_2 dosage on MO decomposition efficiency in the presence of the MIL-53 catalyst. Although MO was completely removed after 90 minutes of the reaction when the concentration of H_2O_2 increased from 0.048 M to 0.288 M, the rate of the MO decomposition reaction varied. It increased as the concentration of H_2O_2 increased from 0.048 M to 0.192 M, while remaining visually unchanged as

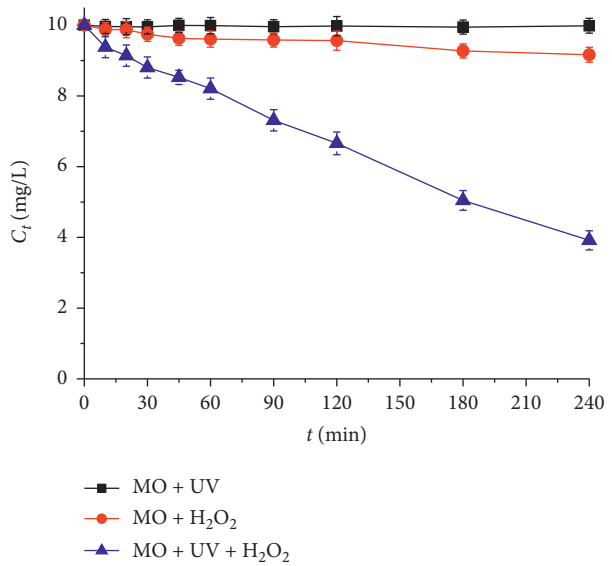

Figure 6: MO decomposition profile under different conditions in the absence of a catalyst (experimental conditions: 0.192 M·H_2O_2; temperature: 30°C).

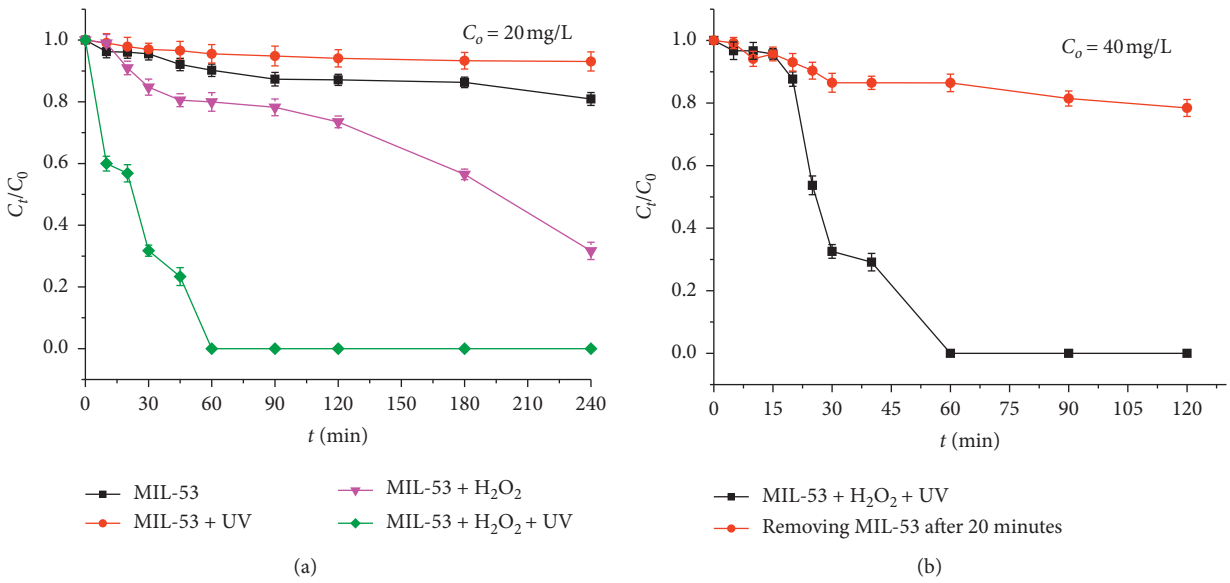

Figure 7: (a) Decomposition profile of MO under different conditions. (b) Leaching experiments (experimental conditions: 0.5 g/L of the catalyst; 0.192 M H_2O_2; temperature: 30°C).

the concentration of H_2O_2 increased to 0.288 M. Therefore, in subsequent experiments, the H_2O_2 dosage used was 2 mL per 100 mL of the MO solution, equivalent to the concentration of 0.192 M H_2O_2, so as not to affect the rate of the MO decomposition reaction.

(3) Effect of Catalyst Dosage. The effect of the amount of the catalyst on MO degradation by UV/H_2O_2 on the MIL-53 catalyst is shown in Figure 10. The results show that MO decomposition efficiency was only ~70% after 120 minutes of the reaction at the catalyst dosage of 0.25 g/L. When the amount of the catalyst increased to 0.5 g/L, the rate of MO decomposition increased significantly, and MO was decomposed completely after 90 minutes of the reaction. The increase in the amount of the catalyst leads to an increase in the number of available adsorbents and the catalyst sites for MO decomposition, so the efficiency of the degradation increases. However, MO degradation was almost constant when the amount of MIL-53 increased from 0.5 g/L to 1.0 g/L, where the number of catalytic sites is given which is completely satisfied for all chemical conversion conditions. Therefore, in subsequent experiments, using of MIL-53 catalyst dosage was 0.5 g/L.

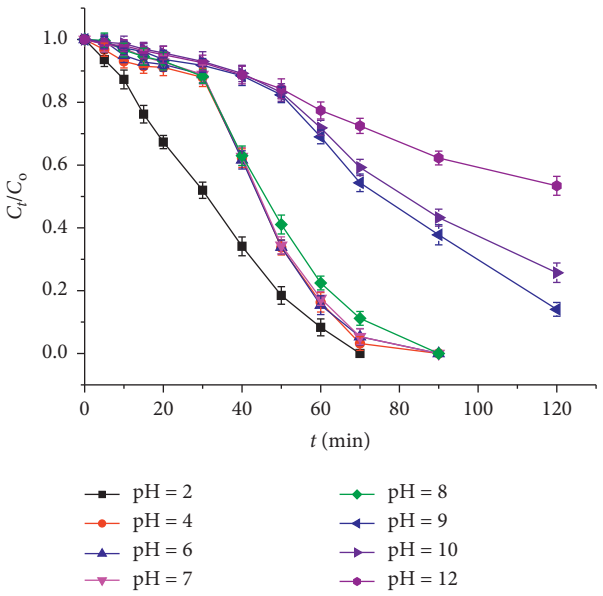

Figure 8: MO degradation by UV/H_2O_2 over the MIL-53 catalyst at different solution pH (experimental condition: 0.5 g/L of the catalyst; 40 mg/L MO; 0.192 M H_2O_2; temperature 30°C; UV radiation).

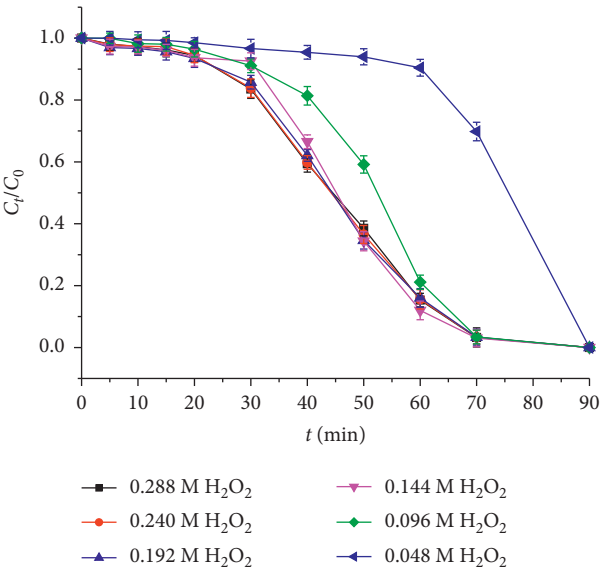

Figure 9: MO degradation profile by the heterogeneous UV/Fenton-like system via the MIL-53 catalyst at different concentrations of H_2O_2 (experimental conditions: 0.5 g/L of the catalyst; 40 mg/L MO; temperature 30°C; UV radiation).

(4) Effect of Initial MO Concentration. Figure 11 shows that when the MO concentration increases from 40 to 60 mg/L, the degradation of MO increases. However, MO degradation almost unchanged when the concentration of MO in the initial solution varied from 60 mg/L to 120 mg/L. The higher amount of MO in the oxidation process on various catalyst systems generally generates a mixture of different products [32, 33]. However, in the case of using the MIL-53 catalyst

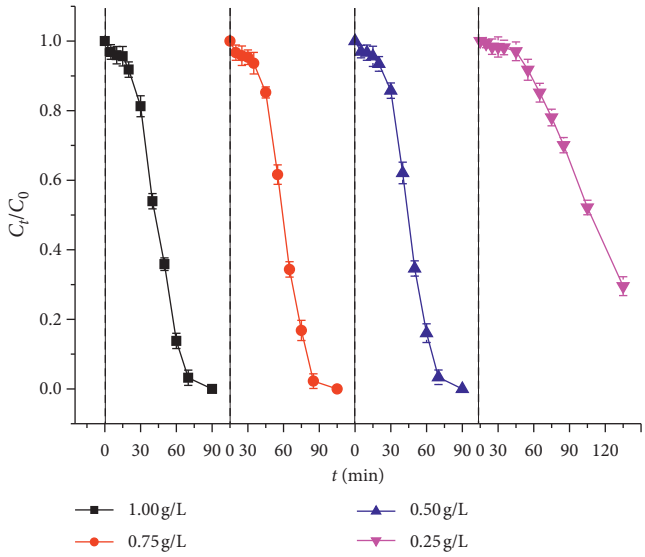

Figure 10: MO decomposition by H_2O_2 on MIL-53(Fe) at different catalyst dosages (experimental conditions: 40 mg/L MO; 0.192 M H_2O_2; temperature 30°C; UV radiation).

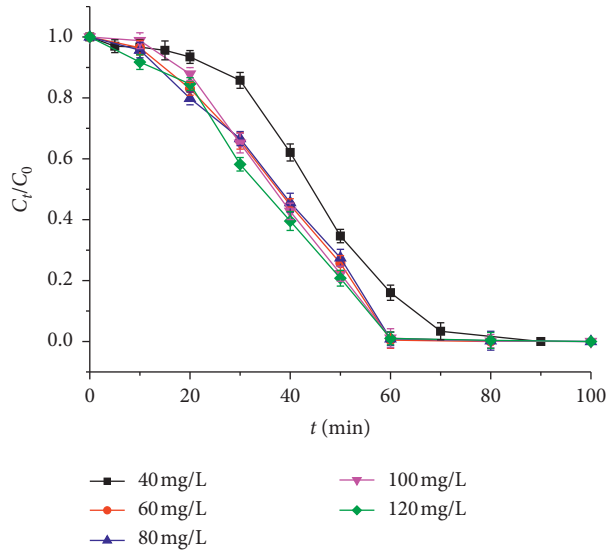

Figure 11: MO decomposition profile by heterogeneous UV/H_2O_2 Fenton-like process using the MIL-53 catalyst at different initial MO concentrations (experimental conditions: 0.5 g/L of the catalyst; 0.192 M·H_2O_2; temperature 30°C; UV radiation).

and under these study reaction conditions, MO oxidation did not produce any other product as evidenced by chromatograms of the reaction mixture after regular time intervals (Figure 12(a)). The peak of MO at the retention time of 4 minutes was no longer observed after 60 minutes of the reaction. The peak at the retention time of 2 minutes is probably the impurity in the original solution. Additionally, Figure 12(b) shows that %TOC reduced to 80% after 100 min. This confirms that MO was completely mineralized into simple substances (H_2O and CO_2) during the treatment process.

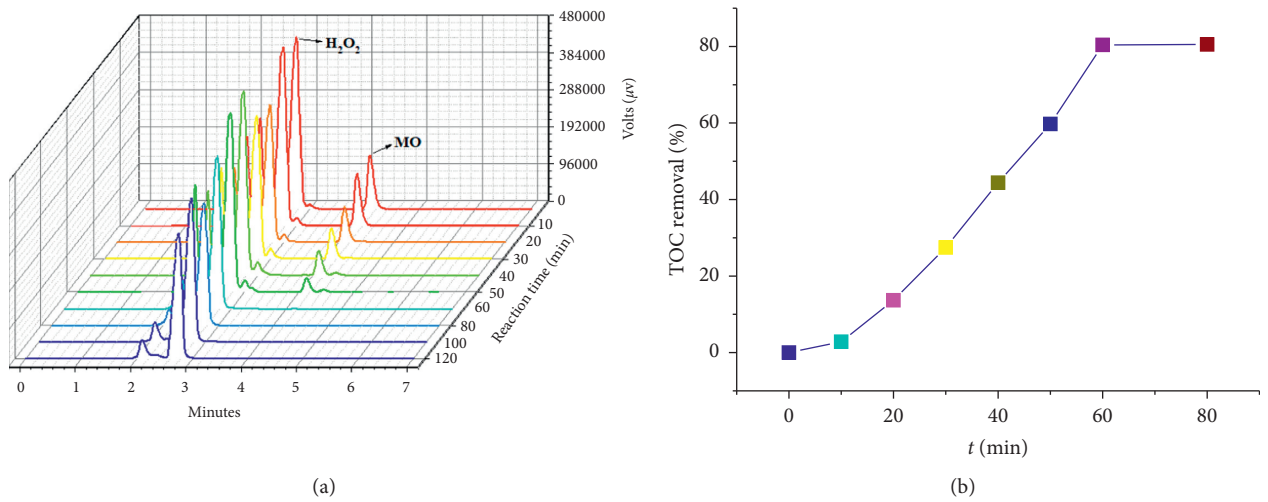

Figure 12: (a) HPLC chromatography and (b) %TOC of the reaction solution containing MO and hydroperoxide at different time intervals (experimental conditions: 0.5 g/L of the catalyst; 60 mg/L MO; 0.192 M·H_2O_2; temperature 30°C; UV radiation).

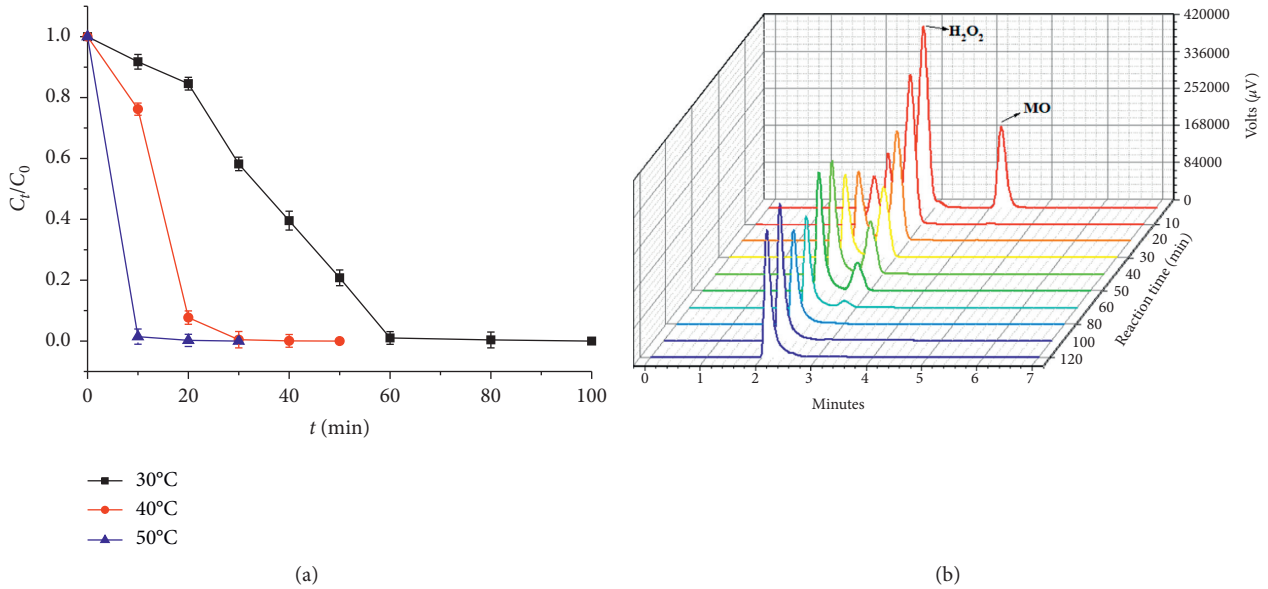

Figure 13: (a) MO decomposition profile using the heterogeneous UV/Fenton-like MIL-53 catalyst at different reaction temperatures; (b) HPLC chromatograms of the reaction solution containing MO and hydroperoxide at 50°C at different reaction times (experimental conditions: 0.5/L g of the catalyst; 120 mg/L MO; 0.192 M H_2O_2; UV radiation).

(5) Effect of Reaction Temperature. The effect of reaction temperature on the efficiency of MO decomposition by the heterogeneous UV/Fenton-like MIL-53 catalyst is shown in Figure 13(a). It is clear that when the reaction temperature increased from 30°C to 50°C, the efficiency of MO decomposition increased significantly when it took less time for MO to be completely decomposed, from 60 minutes at 30°C to only 10 minutes at 50°C. This can be explained by the fact that the rate of H_2O_2 decomposition to produce hydroxyl radicals, strong oxidizing radicals for the MO decomposition, is probably faster at higher temperatures. This is evidenced by the HPLC chromatogram shown in Figure 13(b). Obviously, the peak at retention time of 2.8 minutes, typical for H_2O_2, decreased rapidly with reaction time and disappeared almost completely after 80 minutes of the reaction (the peak at retention time of 2 minutes was probably the impurities present in the original solution as seen in Figure 12(a)).

(6) Kinetic of the MO Decomposition Process. In the kinetic investigation, the H_2O_2 content in the liquid phase was maintained at an excessive level for complete oxidation of MO. Hence, H_2O_2 dependence of the degradation reaction kinetics can be avoided. The degradation kinetics can be represented by the Langmuir–Hinshelwood model in the following equation:

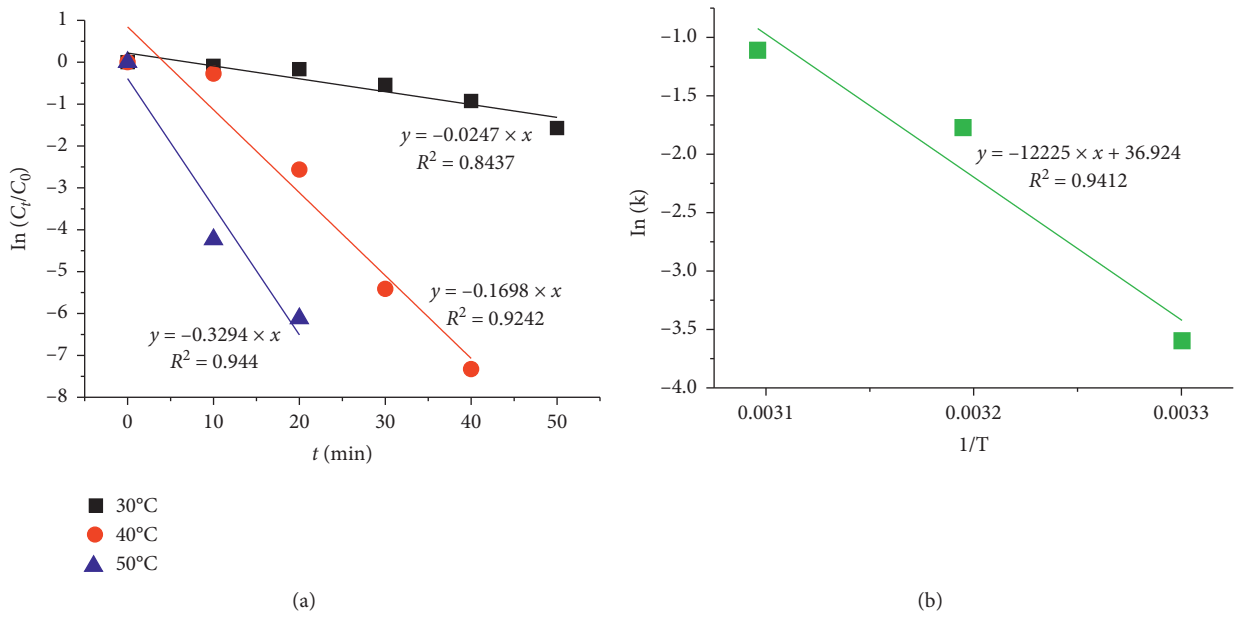

Figure 14: (a) Pseudo-first-order kinetic plots of the degradation of MO by the heterogeneous UV/Fenton-like MIL-53 catalyst at different reaction temperatures; (b) Arrhenius plots.

Table 1: The order rate constants (k) for MO photodegradation of the previous works.

Photodegradation systems	Rate constant (min^{-1})	Temperature (°C)	Initial MO concentration (mg/L)	Catalyst dosage (g/L)	References
UV/H_2O_2/MIL-53	0.0274	30	120	0.5	The present work
UV/H_2O_2/MIL-53	0.1698	40	120	0.5	The present work
UV/H_2O_2/MIL-53	0.3294	50	120	0.5	The present work
TiO_2 powder/UV/H_2O_2	0.003	—	7.8125	1	[34]
TiO_2 doctor blade/UV/H_2O_2	0.001	—	7.8125	1	[34]
β-FeOOH/UV/H_2O_2	0.036	25	80	0.2	[35]
Hydronium jarosite/UV/H_2O_2	0.040	25	80	0.2	[35]
Ammonium jarosite/UV/H_2O_2	0.022	25	80	0.2	[35]

$$\ln\left(\frac{C_t}{C_0}\right) = -kt, \tag{4}$$

where k is the rate constant (min^{-1}) and C_0 and C_t are concentrations at the time $t = 0$ and time t (min), respectively. A plot of ln (C_t/C_0) versus t will yield the reaction rate constant. Figure 14(a) displays such a plot for MIL-53 at different temperatures. The results show that the reaction kinetics is in good agreement with the Langmuir–Hinshelwood model with high coefficient of determination ($R^2 = 0.844$–0.944). k is considered as a rate constant for the pseudo-first-order kinetic reaction. The value of k is widely used to compare how fast or slow a first-order reaction is at a given temperature.

A comparison of the rate constants of the first-order kinetic reaction (k) for MO photodegradation with various catalysts is shown in Table 1. It was found that the value of k for the present study is higher or compatible with previous reports indicating that the heterogeneous UV/Fenton-like process with the MIL-53 catalyst provides the fast reaction kinetics, especially, at the high temperature (40–50°C).

The rate constants observed in Figure 14(a) clearly reflect their dependence on the treatment temperature. Such dependence can be represented by the Arrhenius equation:

$$\ln k = \ln A - \frac{E_a}{\mathrm{RT}}, \tag{5}$$

in which E_a is the activation energy, R is the gas constant, T is the treatment temperature, and A is the frequency of collisions in the correct orientation or frequency factor.

The value of E_a can be determined using a linear plot of ln$k$ versus $1/T$ (Figure 14(b)). E_a is the minimum amount of

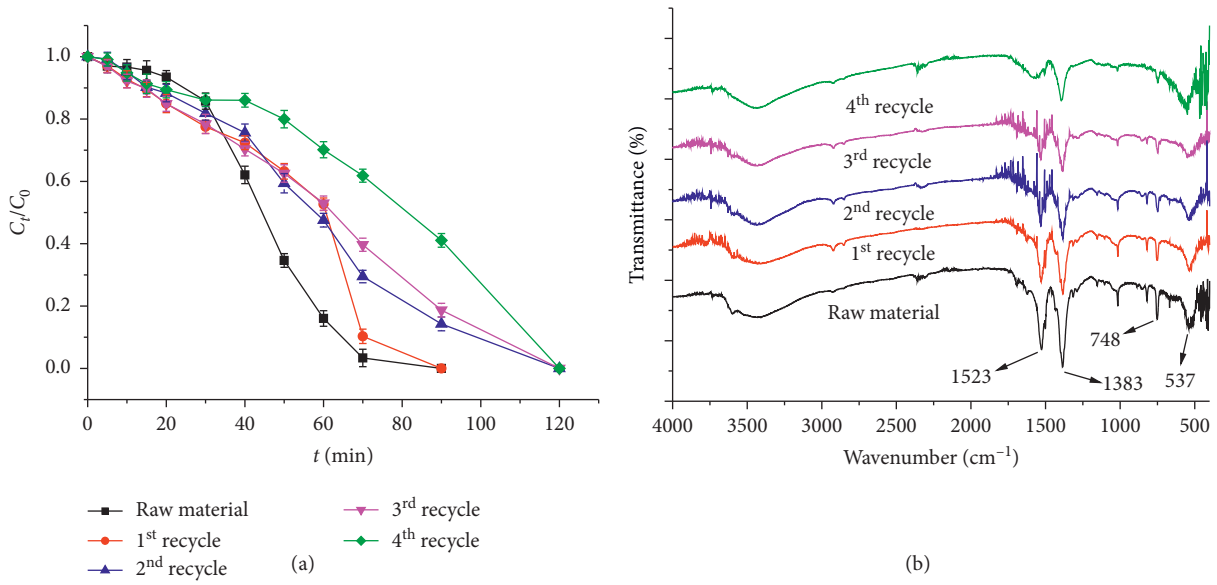

FIGURE 15: (a) MO decomposition profile by heterogeneous UV/Fenton-like reused MIL-53 catalysts; (b) FT-IR spectra of reused MIL-53 samples (experimental conditions: 0.5 g/L of the catalyst; 40 mg/L MO; 0.192 M H_2O_2; temperature: 30°C; UV radiation).

energy required for a reaction to happen. At higher temperatures, the probability of collision between two molecules is higher, which affects the activation energy of a reaction [36]. In this study, the activation energy of 24.3 kcal/mol was found from the plot. This value of E_a confirms that the degradation reaction of MO occurs in the kinetic region (kinetic surface reaction) [16].

(7) Reusability of the MIL-53 Catalyst. After each experiment, the MIL-53 catalyst was filtered, washed with water, and dried for reuse. The results of catalytic activity survey after 5 uses are shown in Figure 15(a). MO degradation by heterogeneous UV/Fenton-like process using reused MIL-53 decreased slightly over time, but MO was completely decomposed after 120 minutes of the reaction.

Comparing the FT-IR spectrum of reused MIL-53 samples and the original sample (Figure 15(b)) reveals that the reused MIL-53 samples still exhibit full characteristic vibration for MIL-53 with absorption bands at 1,523, 1,383, 748, and 537 cm^{-1} [26]. This proves that the MIL-53 catalyst is highly stable under experimental conditions in this study.

4. Conclusions

The MIL-53 material was successfully synthesized by hydrothermal process. It possesses high specific area with highly ordered porous distribution and high crystallinity. MIL-53 could catalyze for UV/Fenton-like degradation of MO. The kinetic data are fitted well with the kinetic model of Langmuir–Hinshelwood. The heterogeneous UV/Fenton-like process using MIL-53 provided the fast reaction kinetics and exhibited good catalytic activity with complete mineralization. This catalyst was stable after four recycles with a slight loss of catalytic activity, which indicates great potential for practical application of the MIL-53 catalyst in treatment of wastewater.

Data Availability

The data used to support the findings of this study are available from the corresponding author upon request.

Conflicts of Interest

The authors declare that they have no conflicts of interest.

References

[1] C. Park, M. Lee, B. Lee et al., "Biodegradation and biosorption for decolorization of synthetic dyes by Funalia trogii," *Biochemical Engineering Journal*, vol. 36, no. 1, pp. 59–65, 2007.

[2] G. Crini, "Non-conventional low-cost adsorbents for dye removal: a review," *Bioresource Technology*, vol. 97, no. 9, pp. 1061–1085, 2006.

[3] T. Panswad and S. Wongchaisuwan, "Mechanisms of dye wastewater colour removal by magnesium carbonate-hydrated basic," *Water Science and Technology*, vol. 18, no. 3, pp. 139–144, 1986.

[4] M. Koch, A. Yediler, D. Lienert, G. Insel, and A. Kettrup, "Ozonation of hydrolyzed azo dye reactive yellow 84 (CI)," *Chemosphere*, vol. 46, no. 1, pp. 109–113, 2002.

[5] P. K. Malik and S. K. Saha, "Oxidation of direct dyes with hydrogen peroxide using ferrous ion as catalyst," *Separation and Purification Technology*, vol. 31, no. 3, pp. 241–250, 2003.

[6] G. Ciardelli, L. Corsi, and M. Marcucci, "Membrane separation for wastewater reuse in the textile industry," *Resources, Conservation and Recycling*, vol. 31, no. 2, pp. 189–197, 2001.

[7] F.-C. Wu and R.-L. Tseng, "High adsorption capacity NaOH-activated carbon for dye removal from aqueous solution," *Journal of Hazardous Materials*, vol. 152, no. 3, pp. 1256–1267, 2008.

[8] H. Lan, A. Wang, R. Liu, H. Liu, and J. Qu, "Heterogeneous photo-fenton degradation of acid red B over Fe2O3 supported on activated carbon fiber," *Journal of Hazardous Materials*, vol. 285, pp. 167–172, 2015.

[9] A. Asghar, A. A. Abdul Raman, and W. M. A. Wan Daud, "Advanced oxidation processes for in-situ production of hydrogen peroxide/hydroxyl radical for textile wastewater treatment: a review," *Journal of Cleaner Production*, vol. 87, pp. 826–838, 2015.

[10] G. Boczkaj and A. Fernandes, "Wastewater treatment by means of advanced oxidation processes at basic pH conditions: a review," *Chemical Engineering Journal*, vol. 320, pp. 608–633, 2017.

[11] Q. Wang, S. Tian, J. Long, and P. Ning, "Use of Fe(II)Fe(III)-LDHs prepared by co-precipitation method in a heterogeneous-fenton process for degradation of methylene blue," *Catalysis Today*, vol. 224, pp. 41–48, 2014.

[12] A. D. Bokare and W. Choi, "Review of iron-free fenton-like systems for activating H_2O_2 in advanced oxidation processes," *Journal of Hazardous Materials*, vol. 275, pp. 121–135, 2014.

[13] F. Martínez, G. Calleja, J. A. Melero, and R. Molina, "Heterogeneous photo-Fenton degradation of phenolic aqueous solutions over iron-containing SBA-15 catalyst," *Applied Catalysis B: Environmental*, vol. 60, no. 3-4, pp. 181–190, 2005.

[14] Y. Huang, C. Cui, D. Zhang, L. Li, and D. Pan, "Heterogeneous catalytic ozonation of dibutyl phthalate in aqueous solution in the presence of iron-loaded activated carbon," *Chemosphere*, vol. 119, pp. 295–301, 2015.

[15] S. Guo, G. Zhang, and J. Wang, "Photo-Fenton degradation of rhodamine B using Fe_2O_3-Kaolin as heterogeneous catalyst: characterization, process optimization and mechanism," *Journal of Colloid and Interface Science*, vol. 433, pp. 1–8, 2014.

[16] D. Q. Khieu, D. T. Quang, T. D. Lam, N. H. Phu, J. H. Lee, and J. S. Kim, "Fe-MCM-41 with highly ordered mesoporous structure and high Fe content: synthesis and application in heterogeneous catalytic wet oxidation of phenol," *Journal of Inclusion Phenomena and Macrocyclic Chemistry*, vol. 65, no. 1-2, pp. 73–81, 2009.

[17] A. K. Dutta, S. K. Maji, and B. Adhikary, "γ-Fe_2O_3 nanoparticles: an easily recoverable effective photo-catalyst for the degradation of rose bengal and methylene blue dyes in the waste-water treatment plant," *Materials Research Bulletin*, vol. 49, pp. 28–34, 2014.

[18] W. Li, Y. Wang, and A. Irini, "Effect of pH and H_2O_2 dosage on catechol oxidation in nano-Fe_3O_4 catalyzing UV-Fenton and identification of reactive oxygen species," *Chemical Engineering Journal*, vol. 244, pp. 1–8, 2014.

[19] M. Anbia and S. Sheykhi, "Synthesis of nanoporous copper terephthalate [MIL-53(Cu)] as a novel methane-storage adsorbent," *Journal of Natural Gas Chemistry*, vol. 21, no. 6, pp. 680–684, 2012.

[20] Y. Bai, G.-J. He, Y.-G. Zhao, C.-Y. Duan, D.-B. Dang, and Q.-J. Meng, "Porous material for absorption and luminescent detection of aromatic molecules in water," *Chemical Communications*, vol. 43, no. 14, p. 1530, 2006.

[21] J.-J. Du, Y.-P. Yuan, J.-X. Sun et al., "New photocatalysts based on MIL-53 metal-organic frameworks for the decolorization of methylene blue dye," *Journal of Hazardous Materials*, vol. 190, no. 1–3, pp. 945–951, 2011.

[22] M. G. Plaza, A. M. Ribeiro, A. Ferreira et al., "Separation of C3/C4 hydrocarbon mixtures by adsorption using a mesoporous iron MOF: MIL-100(Fe)," *Microporous and Mesoporous Materials*, vol. 153, pp. 178–190, 2012.

[23] X. Zhou, H. P. Zhang, G. Y. Wang, Z. G. Yao, Y. R. Tang, and S. S. Zheng, "Zeolitic imidazolate framework as efficient heterogeneous catalyst for the synthesis of ethyl methyl carbonate," *Journal of Molecular Catalysis A: Chemical*, vol. 366, pp. 43–47, 2013.

[24] M. Zhu, D. Srinivas, S. Bhogeswararao, P. Ratnasamy, and M. A. Carreon, "Catalytic activity of ZIF-8 in the synthesis of styrene carbonate from CO_2 and styrene oxide," *Catalysis Communications*, vol. 32, pp. 36–40, 2013.

[25] J. Jia, F. Xu, Z. Long, X. Hou, and M. J. Sepaniak, "Metal-organic framework MIL-53(Fe) for highly selective and ultrasensitive direct sensing of MeHg+," *Chemical Communications*, vol. 49, no. 41, pp. 4670–4672, 2013.

[26] R. Liang, F. Jing, L. Shen, N. Qin, and L. Wu, "MIL-53(Fe) as a highly efficient bifunctional photocatalyst for the simultaneous reduction of Cr(VI) and oxidation of dyes," *Journal of Hazardous Materials*, vol. 287, pp. 364–372, 2015.

[27] L. Ai, L. Li, C. Zhang, J. Fu, and J. Jiang, "MIL-53(Fe): a metal-organic framework with intrinsic peroxidase-like catalytic activity for colorimetric biosensing," *Chemistry-A European Journal*, vol. 19, no. 45, pp. 15105–15108, 2013.

[28] Y. Wang, K. Kretschmer, J. Zhang, A. K. Mondal, X. Guo, and G. Wang, "Organic sodium terephthalate@graphene hybrid anode materials for sodium-ion batteries," *RSC Advances*, vol. 6, no. 62, pp. 57098–57102, 2016.

[29] J. Cui, L. Wang, Y. Han et al., "ZnO nano-cages derived from ZIF-8 with enhanced anti mycobacterium-tuberculosis activities," *Journal of Alloys and Compounds*, vol. 766, pp. 619–625, 2018.

[30] T. A. Vu, G. H. Le, C. D. Dao et al., "Arsenic removal from aqueous solutions by adsorption using novel MIL-53(Fe) as a highly efficient adsorbent," *RSC Advances*, vol. 5, no. 7, pp. 5261–5268, 2015.

[31] A. BabuPonnusami and K. Muthukumar, "A review on fenton and improvements to the fenton process for wastewater treatment," *Journal of Environmental Chemical Engineering*, vol. 2, no. 1, pp. 557–572, 2014.

[32] C. Baiocchi, M. C. Brussino, E. Pramauro, A. B. Prevot, L. Palmisano, and G. Marcì, "Characterization of methyl orange and its photocatalytic degradation products by HPLC/UV-VIS diode array and atmospheric pressure ionization quadrupole ion trap mass spectrometry," *International Journal of Mass Spectrometry*, vol. 214, no. 2, pp. 247–256, 2002.

[33] Y. He, F. Grieser, and M. Ashokkumar, "The mechanism of sonophotocatalytic degradation of methyl orange and its products in aqueous solutions," *Ultrasonics Sonochemistry*, vol. 18, no. 5, pp. 974–980, 2011.

[34] L. Andronic, S. Manolache, and A. Duta, "Photocatalytic degradation of methyl orange: influence of H2O2 in the TiO2-based system," *Journal of Nanoscience and Nanotechnology*, vol. 8, no. 2, pp. 728–732, 2008.

[35] Z. Xu, J. Liang, and L. Zhou, "Photo-fenton-like degradation of azo dye methyl orange using synthetic ammonium and hydronium jarosite," *Journal of Alloys and Compounds*, vol. 546, pp. 112–118, 2013.

[36] H.-Y. Xu, Y. Wang, T.-N. Shi et al., "Heterogeneous fenton-like discoloration of methyl orange using Fe3O4/MWCNTs as catalyst: kinetics and fenton-like mechanism," *Frontiers of Materials Science*, vol. 12, no. 1, pp. 34–44, 2018.